Mode Conversion Caused by Diameter Changes of a Round Dielectric Waveguide

By DIETRICH MARCUSE and RICHARD M. DEROSIER

This paper presents the theory of mode conversion and radiation losses of the lowest order circular electric mode in a dielectric rod (fiber) waveguide and its confirmation by a microwave experiment. The theoretical results were obtained from a theory whose detailed development has been presented in an earlier paper.

The microwave experiment was carried out at approximately 50 GHz. The optical fiber with imperfect walls was simulated by a teflon rod of 1 cm diameter and 1 m length with a periodically corrugated wall.

Mode conversion was observed in excellent agreement with theory. The observed radiation losses are somewhat less than the prediction of the perturbation theory, but the agreement is quite good. The direction and width of the far-field radiation pattern was observed in agreement with theory.

I. INTRODUCTION

A theory of mode conversion and radiation losses of a guided mode in a dielectric slab was described in Ref. 1. The power conversion to spurious guided modes as well as to the continuum of unguided radiation modes was assumed to be caused by deviations from perfect straightness of the air-dielectric interface of the slab. The model of the dielectric slab waveguide was chosen for its simplicity.

Even though the dielectric slab exhibits all the relevant features of mode conversion caused by surface roughness and allows one to draw conclusions as to the order of magnitude of the losses suffered by guided modes in dielectric waveguides of other geometries, it is desirable to report the calculations for a round dielectric rod. The results of calculations for the dielectric rod are directly applicable to light transmission along optical fibers. Furthermore, we wanted to test the predictions of the theory at microwave frequencies where a controlled

experiment, to check the effect of surface imperfections on mode guidance, is feasible. We present in this paper the theoretical treatment of the round dielectric waveguide with wall imperfections and its confirmation by a microwave experiment.

The mode conversion theory of round dielectric waveguides is only sketched in this paper since the basic method of calculation has already been described elsewhere.[1] The theory is simplified by limiting the discussion to circular electric modes. In order to avoid coupling between the circular symmetric and other modes, we assume that the symmetry of the rod is such that all derivatives with respect to the angle φ of a cylindrical polar coordinate system (r, φ, z) vanish $(\partial/\partial\varphi = 0)$.

We conclude again (as in Ref. 1) that the radiation and mode conversion losses caused by deviation of the waveguide walls from perfect straightness are extremely severe, imposing strict tolerance requirements on the fabrication of low loss optical fiber transmission lines.

To confirm the basic aspects of our theory we conducted a microwave experiment. Because of the ready availability of equipment, the frequency range of 50 GHz was chosen. Two teflon rods were used to simulate optical fibers. Both rods had 1 cm diameters and a length of 1 m. One rod was smooth and was used for calibration and reference purposes, while the other rod was machined with periodic grooves to simulate an optical fiber with wall imperfections (Fig. 1).

The periodic wall perturbations cause two guided modes to be coupled together. In fact, it is possible to obtain complete power conversion between these two coupled modes. We have observed complete power conversion in agreement with our theory.

In a certain frequency interval, the periodic grooves cause coupling to the continuous spectrum of radiation modes of the dielectric rod. The measured results are somewhat lower than the theoretical prediction. The reason for this discrepancy can be partly explained by a
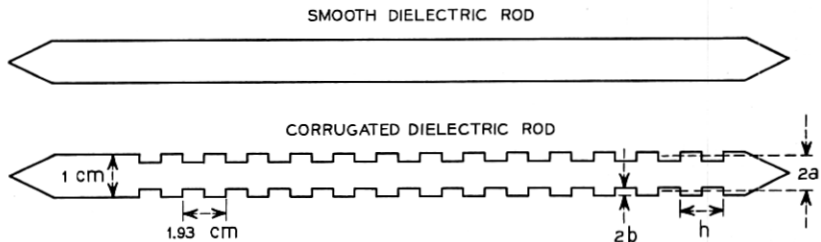

Fig. 1 — The smooth and corrugated teflon rods used for the microwave experiment $(n_g^2 = 2.05)$.

certain ambiguity in the value of the effective radius of the corrugated rod. If we make the assumption that the effective radius is either the largest or smallest radius of our rod, we obtain two curves which bracket our experimental results. However, our experimental values are consistently lower than the theoretical predictions based on an average diameter which is the arithmetic mean of the largest and smallest rod diameter. It is more likely, therefore, that the loss prediction of the perturbation theory is slightly too large for losses which are as high as those which occurred in our experiment.

Our theory also predicts the far-field radiation pattern caused by a strictly periodic wall perturbation.[2] We have observed the peak of the far-field radiation lobe and its width in agreement with theory.

II. TE MODES OF THE DIELECTRIC ROD[3]

Imposing the condition

$$\frac{\partial}{\partial\varphi} = 0, \tag{1}$$

the transverse electric field is composed of the components

$$E_{\varphi}, H_r, H_z. \tag{2}$$

The guided modes have the following form (normal modes of the perfect waveguide are indicated by script letters)

$$\mathcal{E}_{\varphi} = A_n J_1(\kappa_n r) e^{i(\omega t - \beta_n z)} \quad \text{for} \quad r < a \tag{3a}$$

$$\mathcal{E}_{\varphi} = A_n \frac{J_1(\kappa_n a)}{H_1^{(1)}(i\gamma_n a)} H_1^{(1)}(i\gamma_n r) e^{i(\omega t - \beta_n z)} \quad \text{for} \quad r > a. \tag{3b}$$

The two magnetic field components are obtained from the E_{φ} component

$$\mathcal{H}_r = -\frac{i}{\omega\mu} \frac{\partial E_{\varphi}}{\partial z} \tag{4a}$$

$$\mathcal{H}_z = \frac{i}{\omega\mu} \frac{1}{r} \frac{\partial}{\partial r} (rE_{\varphi}). \tag{4b}$$

The various symbols used in these equations have the meanings:

a = radius of the dielectric rod,
β_n = propagation constant of mode n,
$\kappa_n = (n_g^2 k^2 - \beta_n^2)^{\frac{1}{2}},$ \hfill (5)
$\gamma_n = (\beta_n^2 - k^2)^{\frac{1}{2}},$ \hfill (6)
$k = 2\pi/\lambda_0$ = free space propagation constant,

n_g = index of refraction of the waveguide (rod),

ω = radian frequency,

J_1 = Bessel function of order 1, and

$H_1^{(1)}$ = Hankel function of first kind and order 1.

The boundary conditions, requiring that the field components $\mathcal{E}_\varphi$ and $\mathcal{H}_z$ are continuous at $r = a$, lead to the eigenvalue equation for β

$$\frac{\gamma_n}{\kappa_n} \frac{J_1(\kappa_n a)}{J_0(\kappa_n a)} = -i \frac{H_1^{(1)}(i\gamma_n a)}{H_0^{(1)}(i\gamma_n a)}. \tag{7}$$

The subscript 0 designates the Bessel and Hankel functions of zero order. It is convenient to express the mode amplitude A_n by the actual power carried by each mode:

$$P_n = -\frac{1}{2} \int_0^\infty dr \int_0^{2\pi} d\varphi\, r\, \mathcal{E}_\varphi \mathcal{H}_r^* = \pi \frac{\beta_n}{\omega\mu} \int_0^\infty r \mid \mathcal{E}_\varphi \mid^2 dr. \tag{8}$$

The modes will be normalized to the same amount of power (1 watt, for example) so that we write

$$P_n = P. \tag{9}$$

The mode amplitude can now be expressed as

$$A_n^2 = \frac{2\omega\mu}{\pi a^2 \beta_n} \frac{P}{\left(1 + \frac{\kappa_n^2}{\gamma_n^2}\right) \mid J_0(\kappa_n a) J_2(\kappa_n a) \mid}. \tag{10}$$

The modes of the continuous spectrum are given by the expressions

$$\mathcal{E}_\varphi = B J_1(\sigma r) e^{i(\omega t - \beta z)} \qquad r < a \tag{11a}$$

$$\mathcal{E}_\varphi = [C J_1(\rho r) + D N_1(\rho r)] e^{i(\omega t - \beta z)} \qquad r > a. \tag{11b}$$

The two magnetic components are again obtained from equations (4a) and (4b). N_1 is the Neumann function of order 1 and the parameters σ and ρ are defined:

$$\sigma = (n_g^2 k^2 - \beta^2)^{\frac{1}{2}}, \qquad \rho = (k^2 - \beta^2)^{\frac{1}{2}}. \tag{12}$$

The normalization of the continuous modes involves the Dirac δ-function

$$P\delta(\rho - \rho') = \pi \frac{\beta}{\omega\mu} \int_0^\infty r E_\varphi(\rho) E_\varphi^*(\rho') \, dr. \tag{13}$$

The boundary conditions at $r = a$ determine the relations between the constants C, D, and B

$$\frac{C}{B} = \frac{\pi}{2} \rho a \left(J_1(\sigma a) N_0(\rho a) - \frac{\sigma}{\rho} J_0(\sigma a) N_1(\rho a) \right) \tag{14a}$$

$$\frac{D}{B} = -\frac{\pi}{2} \rho a \left(J_1(\sigma a) J_0(\rho a) - \frac{\sigma}{\rho} J_0(\sigma a) J_1(\rho a) \right), \tag{14b}$$

and these coefficients can be expressed in terms of the power carried by the mode

$$P = \pi \frac{\beta}{\rho \omega \mu} (C^2 + D^2). \tag{15}$$

The actual field of a dielectric rod with imperfect walls can be expanded in terms of the normal modes of the perfect rod:

$$E_\varphi = \sum_{n=0}^{\infty} C_n \mathcal{E}_n + \int_0^\infty g(\rho) \mathcal{E}(\rho) \, d\rho. \tag{16}$$

The remaining caluclation of the power loss to radiation and guided modes, as well as the energy exchange phenomena between different guided modes, are exactly analogous to those developed in Ref. 1 so that their derivation need not be repeated here. In Section III we simply quote the results of the corresponding calculations.

III. SINUSOIDAL WALL PERTURBATION

It was pointed out in Ref. 1 that a sinusoidal wall perturbation can couple only those two modes whose beat wavelength

$$\Lambda_n = \frac{2\pi}{\beta_0 - \beta_n} \tag{17}$$

coincides with the mechanical period h of the wall perturbation. It is therefore possible to consider the coupling phenomenon between only two modes with the result that the coefficient C_0 of the incident mode and the coefficient C_1 of one of the spurious modes obey the relations

$$C_0(z) = \cos |\kappa_{01}| z \tag{18a}$$

$$C_1(z) = \left(\frac{\kappa_{01}^*}{\kappa_{01}} \right)^{\frac{1}{2}} \sin |\kappa_{01}| z \tag{18b}$$

with

$$
a\kappa_{01} = \frac{(n_v^2 - 1)\dfrac{A_0}{a}(ka)^2}{2a(\beta_0\beta_1)^{\frac{1}{2}}}
$$
$$
\cdot \frac{J_1(\kappa_0 a)J_1(\kappa_1 a)}{\left[\left(1 + \dfrac{\kappa_0^2}{\gamma_0^2}\right)\left(1 + \dfrac{\kappa_1^2}{\gamma_1^2}\right)J_0(\kappa_0 a)J_0(\kappa_1 a)J_2(\kappa_0 a)J_2(\kappa_1 a)\right]^{\frac{1}{2}}} \cdot \tag{19}
$$

Here, A_0 is the amplitude of the sinusoidal wall deflection

$$
\left.\begin{aligned}
r(z) &= a - A_0 \sin \theta z \\
\theta &= \beta_0 - \beta_1
\end{aligned}\right\} . \tag{20}
$$

The microwave experiment was conducted with a teflon rod with meandering grooves cut into it. The depth of the grooves is given by $2b$ as shown in Fig. 1. The amplitude of the fundamental Fourier component of the periodic wall deflection of Fig. 1 is given by

$$
A_0 = \frac{4b}{\pi} . \tag{21}
$$

The two modes exchange their power completely over a distance

$$
D = \frac{\pi}{2 \mid \kappa_{01} \mid} . \tag{22}
$$

The radiation loss of the dielectric waveguide of Fig. 1 can be calculated by the methods of Ref. 1 resulting in the following equation.

$$
\frac{\Delta P}{P} = \frac{L}{a} \frac{4(n_v^2 - 1)^2 \left(\dfrac{b}{a}\right)^2 (ka)^4}{\pi\beta_0 a}
$$
$$
\cdot \frac{J_1^2(\kappa_0 a)}{\left(1 + \dfrac{\kappa_0^2}{\gamma_0^2}\right) \mid J_0(\kappa_0 a)J_2(\kappa_0 a) \mid} \sum_{m=0}^{N} \frac{J_1^2(\sigma_m a)}{(2m + 1)^2\left[\left(\dfrac{C_m}{B_m}\right)^2 + \left(\dfrac{D_m}{B_m}\right)^2\right]} \cdot \tag{23}
$$

ΔP is the power lost to radiation modes on a section of the waveguide of length L, and P is the power of the incident lowest order circular electric mode. The meaning of a and b is explained in Fig. 1. The sum in equation (23) takes account of the contributions of each component of the Fourier expansion of the distorted wall profile. The Fourier amplitudes of the function shown in Fig. 2 are

$$
A_m = \frac{4b}{\pi(2m + 1)} \tag{24}
$$

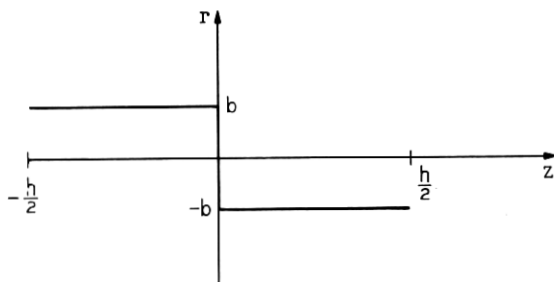[the zero component of this expansion appeared already in equation

Fig. 2 — The wall distortion function with Fourier expansion:

$$r = \sum_{m=0}^{\infty} \frac{4b}{(2m+1)\pi} \sin\left[(2m+1)\frac{2\pi}{h}z\right]$$

(21)]. The index m, which has been added to the coefficients B, C, and D appearing in equations (14a and b) indicates that they must be evaluated for the following values of

$$\beta_m = \beta_0 - (2m+1)\frac{2\pi}{d}, \tag{25a}$$

$$\sigma_m = (n_o^2 k^2 - \beta_m^2)^{\frac{1}{2}}, \tag{25b}$$

$$\rho_m = (k^2 - \beta_m^2)^{\frac{1}{2}}. \tag{25c}$$

The physical reason for the occurence of these discrete values of the propagation constant β in the continuous spectrum of modes is the requirement (derived in Ref. 1) that only those values of β are appreciably coupled to the incident guided mode which satisfy the relation

$$\beta_0 - \beta = \frac{2\pi}{\Lambda_m} \tag{26}$$

where Λ_m is the period length of a Fourier component of the wall distortion function.

IV. THE STATISTICAL CASE

To first order of perturbation theory, the expansion coefficient $g(\rho, z)$ appearing in equation (16) is given by

$$g(\rho, z) = L \frac{k^2(n_o^2 - 1)(\rho)^{\frac{1}{2}}}{(2)^{\frac{1}{2}}i(\beta_0\beta)^{\frac{1}{2}}}$$

$$\cdot \frac{\varphi J_1(\kappa_0 a)J_1(\sigma a)}{\left\{\left[\left(\frac{C}{B}\right)^2 + \left(\frac{D}{B}\right)^2\right]\left(1 + \frac{\kappa_0^2}{\gamma_0^2}\right) \mid J_0(\kappa_0 a)J_2(\kappa_0 a)\mid\right\}^{\frac{1}{2}}} \tag{27}$$

with

$$\varphi = \frac{1}{L} \int_0^L [f(z) - a]e^{-i(\beta_0 - \beta)z} \, dz. \tag{28}$$

It was pointed out in Ref. 1 that the average power loss caused by scattering into the radiation field is given by

$$\left\langle \frac{\Delta P}{P} \right\rangle_{av} = \int_{-k}^{k} \langle |g|^2 \rangle_{av} \frac{\beta}{\rho} \, d\beta. \tag{29}$$

The symbol $\langle \ \rangle_{av}$ indicates an ensemble average. The ensemble average of $|\varphi|^2$ is given by

$$\langle |\varphi|^2 \rangle_{av} \approx \frac{2}{L} \int_0^L R(u) \cos(\beta_0 - \beta_m)u \, du \tag{30}$$

with the correlation function

$$R(u) = \langle [f(z) - a][f(z + u) - a] \rangle_{av}. \tag{31}$$

The relative power loss caused by radiation from the rod is obtained from equations (27) and (29)

$$\frac{1}{L} \left\langle \frac{\Delta P}{P} \right\rangle_{av} = \frac{k^4(n_g^2 - 1)^2}{2\beta_0 \left(1 + \frac{\kappa_0^2}{\gamma_0^2}\right)} \frac{J_1^2(\kappa_0 a)}{|J_0(\kappa_0 a)J_2(\kappa_0 a)|} \int_{-k}^{k} \frac{[\langle |\varphi|^2 \rangle_{av} L]J_1^2(\sigma a)}{\left(\frac{C}{B}\right)^2 + \left(\frac{D}{B}\right)^2} \, d\beta. \tag{32}$$

V. NUMERICAL RESULTS FOR THE STATISTICAL CASE

To be able to make numerical predictions, let us assume that the correlation function is given by

$$R(u) = A^2 \exp\left(-\frac{|u|}{B}\right) \tag{33}$$

so that we obtain

$$L\langle |\varphi|^2 \rangle_{av} = \frac{2A^2}{B} \frac{1}{(\beta_0 - \beta)^2 + \frac{1}{B^2}}. \tag{34}$$

Figure 3 shows a plot of $(a^3/LA^2)(\Delta P/P)$ as a function of B/a for $n_g = 1.01$, $ka = 23.0$ and $n_g = 1.5$, $ka = 3.0$. Both conditions are chosen so that only the lowest order circular electric mode can propagate in the dielectric rod.

To get a feeling for the magnitude of the losses to be expected from random variations of the rod's radius, we calculate the rms deviation
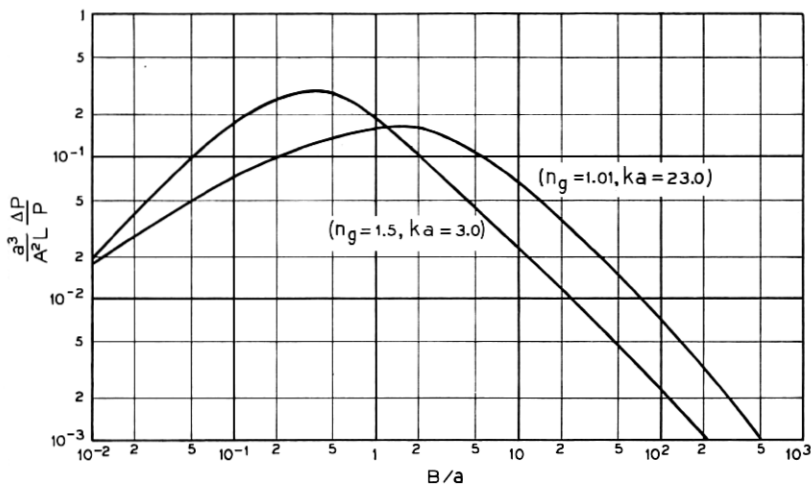
Fig. 3 — Normalized radiation loss caused by random wall perturbations with exponential correlation function, a = radius of fiber, A = rms value of wall deviation, L = length of waveguide section, k = free space propagation constant. The dimensions shown in the figure were chosen to ensure single guided mode operation.

A required to cause $\Delta P/P = 0.1$ for a rod length of $L = 1$ cm for $n_g = 1.01$ and the worst possible value of $B/a = 2$. Assuming $\lambda = 1\mu$ we get from $ka = 23$ the value $a = 3.66\mu$ for the guide radius. With (from Fig. 3)

$$\frac{a^3}{A^2 L} \frac{\Delta P}{P} = 0.16$$

we find

$$\frac{A}{a} = 1.5 \times 10^{-2} = 1.5\%$$

or

$$A = 550 \text{ Å}.$$

As discussed in Ref. 1, it may be permissible to apply the perturbation calculation of the radiation loss repeatedly so that from

$$\frac{\Delta P}{P} = -\alpha z, \tag{35}$$

$$P = P_0 e^{-\alpha L} \tag{36}$$

can be obtained. We can then ask for the rms deviation A of the rod's radius which causes a loss of 10 dB/km. With the numerical values used above we find

$$A = 8.4 \text{ Å}.$$

Almost the same figure was obtained for the rms deviation of the half width of the dielectric slab which causes a 10 dB/km radiation loss of the lowest order (even) guided mode. However, in the case of the slab, one wall was assumed to be perfect.

VI. THE MICROWAVE EXPERIMENT

The experimental setup is shown in Fig. 4. The microwave signal is generated by a reflex klystron whose rectangular waveguide output is fed into a round waveguide by means of a rectangular-to-round waveguide transducer. The round waveguide is connected to a section of round helix waveguide which serves as a mode filter suppressing all but the circular electric $TE_{01}^{(m)}$ mode. Transition between the $TE_{01}^{(m)}$ mode of the round waveguide and the corresponding TE_{01} mode of the dielectric rod waveguide is achieved by inserting the rod into the waveguide. This mode launcher is not perfect since a small amount of TE_{02} mode of the dielectric waveguide is excited. The $TE_{01}^{(m)}$ mode of the round waveguide cannot excite the pure TE_{01} mode of the dielectric rod since the field configurations of the two modes are slightly different. In addition to some residual TE_{02} mode, small amounts of asymmetric modes of the dielectric rod are also excited because of imperfect centering of the rod inside the round waveguide.

To probe the field outside of the dielectric rod and detect the conversion of power from the TE_{01} to the TE_{02} mode, we used a probe which
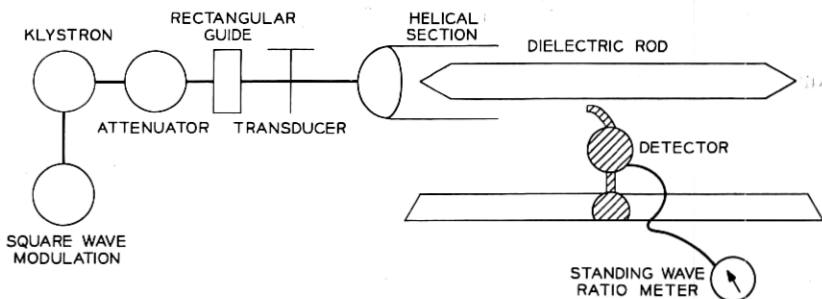
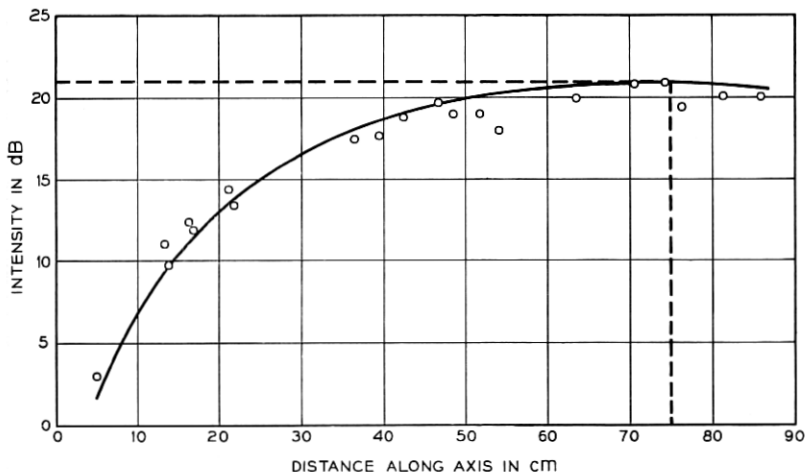

Fig. 4 — Block diagram of the microwave experiment.

Fig. 5 — Buildup of the TE$_{02}$ mode along the corrugated rod. Groove depth = 7.6×10^{-3} cm.

consisted simply of an L-shaped piece of RG 98U waveguide which was mounted on an optical rail, which made it possible to move the detector parallel to the dielectric rod. The receiver attached to the L-shaped probe consisted of a single diode detector followed by an amplifier which was tuned to 250 Hz. The klystron was amplitude modulated at that same frequency. The periodicity of the grooves of the corrugated dielectric rod (Fig. 1) was chosen equal to the beat wavelength between the TE$_{01}$ and TE$_{02}$ modes of the dielectric rod as given by equation (17).

Mode conversion from TE$_{01}$ to the TE$_{02}$ mode can easily be observed with our detector arrangement because the TE$_{02}$ mode extends much farther away from the rod than the more tightly confined TE$_{01}$ mode. Moving the detector to approximately 4 mm from the surface of the rod made it impossible to observe any trace of the TE$_{01}$ mode, while the TE$_{02}$ mode could easily be detected.

That the corrugation does indeed serve to transfer power from the TE$_{01}$ to the TE$_{02}$ mode is shown in Fig. 5. The measured values of TE$_{02}$ power are shown as dots on this figure. Also shown is a plot of the $\sin^2 x$ function which gives the theoretical law of the power increase according to equation (18b). The slight scatter of the measured points is caused by interference between the TE$_{02}$ mode and some other residual mode which is unintentionally generated by the mode launcher. From equation (22) we calculate $D = 80$cm for our particular experiment. From Fig. 5 we see that the experimental value of the total energy ex-

change length is approximately 75 cm. The remaining discrepancy between the theoretical and experimental values can easily be attributed to the machining accuracy of the rod which was no better than 2.5×10^{-3} cm. Striking proof of the identity of the mode whose buildup is shown in Fig. 5 is provided by Fig. 6.

Figure 6 was obtained by moving the L-shaped detector transversely at the end of either the smooth or the corrugated rod. The detector is thus probing the near field radiation pattern which results as the guided mode leaves the end of the rod and radiates into space. This near field radiation pattern is a faithful reproduction of the shape of the guided mode inside of the waveguide. The solid curve shown in Fig. 6 was obtained by probing the transverse field pattern of the smooth rod. This field pattern shows clearly the TE_{01} mode. There is a slight distortion in the wings of this mode which is caused by interference between the TE_{01} mode and a small amount of TE_{02} power launched by the transducer. The dotted curve in Fig. 6 was obtained by placing the detector at the end of the corrugated rod. We took care to insert the corrugated
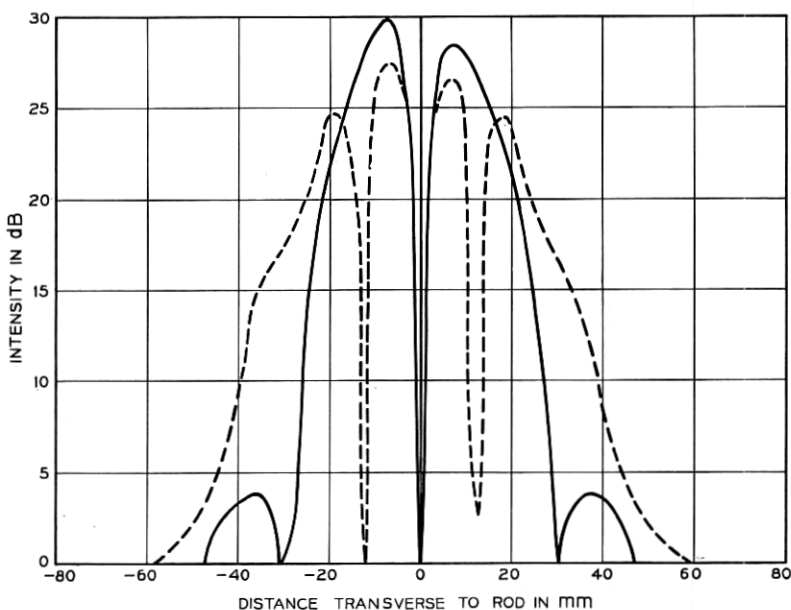

Fig. 6 — The near-field radiation patterns of the guided modes (transverse field distribution). Solid line = TE_{01} mode at end of smooth rod; dotted line = TE_{02} mode at end of corrugated rod.
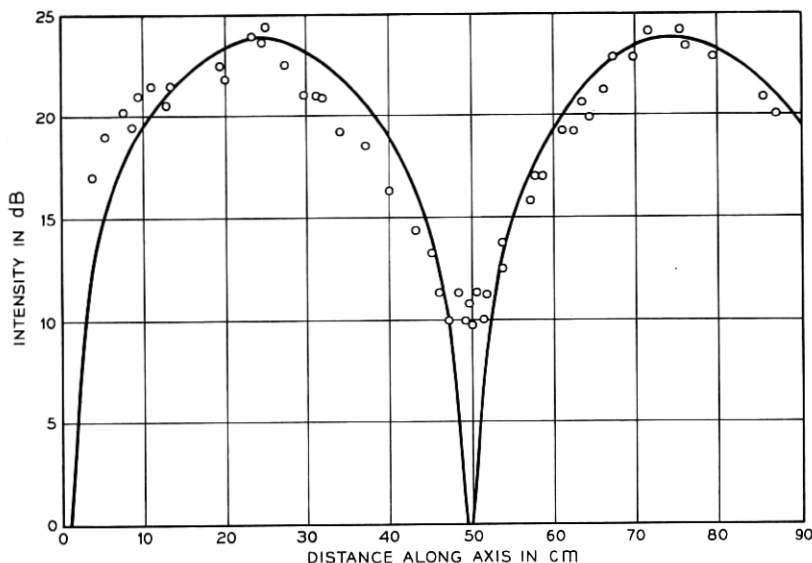
Fig. 7 — Buildup of TE_{02} mode along the corrugated rod. Groove depth $= 2.3 \times 10^{-2}$ cm.

rod so far into the launcher that the section protruding from the launcher was equal to the total power exchange length shown in Fig. 5. It is apparent that the TE_{02} mode (instead of the TE_{01} mode generated by the launcher) is present at the output end of the corrugated rod. It is also apparent that almost complete mode conversion has taken place. Figures 5 and 6 were obtained from a corrugated rod whose grooves had a depth of 7.6×10^{-3} cm. In order to be able to observe radiation losses, we deepened the grooves in this rod to a depth of 2.3×10^{-2} cm. The power buildup as a result of mode conversion from TE_{01} to TE_{02} on the rod with deeper grooves is shown in Fig. 7. The TE_{02} mode is shown to go through two complete power exchanges. The exchange length is now 25 cm in agreement with theory.

Finally, we observed the radiation of power from the corrugated rod with the deeper grooves. Equation (26) indicates the relation between the z-component of the propagation vector of those radiation modes that couple to the TE_{01} mode and the period of the periodic corrugation of the rod. It is clear that the basic Fourier component with length Λ_0 of the corrugated wall distortion function will contribute predominantly to radiation loss. Furthermore, since $\beta < k$ is required for all radiation modes, we see that only very little power can be lost to radia-

tion unless the relation

$$\beta_0 - k \leqq \frac{2\pi}{\Lambda_0} \tag{37}$$

is satisfied. It follows from equation (37) that above $f = 51\text{GHz}$ very little radiation loss is to be expected. Indeed we see in Fig. 7 that complete energy exchange between two guided modes is taking place which would be impossible if substantial amounts of power had been lost to radiation. However, below 51 GHz, equation (23) predicts considerable radiation loss.

The applicability of the radiation loss theory to our experiment is somewhat questionable. We must not forget that equation (23) was derived from a perturbation theory under the assumption that only very little power is lost from the original guided mode. If the radiation detaches itself from the rod over a distance for which the power loss of the guided mode due to radiation is only slight, we may be justified in making the transition to equation (36). However, this procedure becomes more and more questionable as the radiation losses increase. Furthermore, the transition to equation (36) is less likely to be accurate if the radiation is directed forward along the rod. It is shown in Ref. 2 that forward radiation results close to the region where the equal sign of equation (37) applies.

Finally, there is some uncertainty what value "a" for the rod's radius should be used in equation (23). Since the radius of the corrugated rod is variable, some suitable average value must be taken. Figure 8 shows three theoretical curves. The two dotted curves were calculated using the largest and smallest value of the radius in equation (23). The solid curve was obtained by using the average value of the radius. The crosses in Fig. 8 show the results of our loss measurements. It is apparent that most of these points fall within the two dotted curves. However, all points lie below the solid curve. These loss measurements were obtained by comparing the output power at the end of the smooth and corrugated rod. The accuracy of these measurements is no better than approximately $\pm\frac{1}{2}$ dB. In view of the discussion of the applicability of the perturbation theory to high radiation losses, the agreement between theory and experiment must be considered as good.

Figure 9 shows the angle of the far-field pattern of the radiation lobes caused by power loss due to the corrugated wall. The dots are measured values, while the curve is a result of the theory of Ref. 2. Again we see good agreement between experiment and theory.
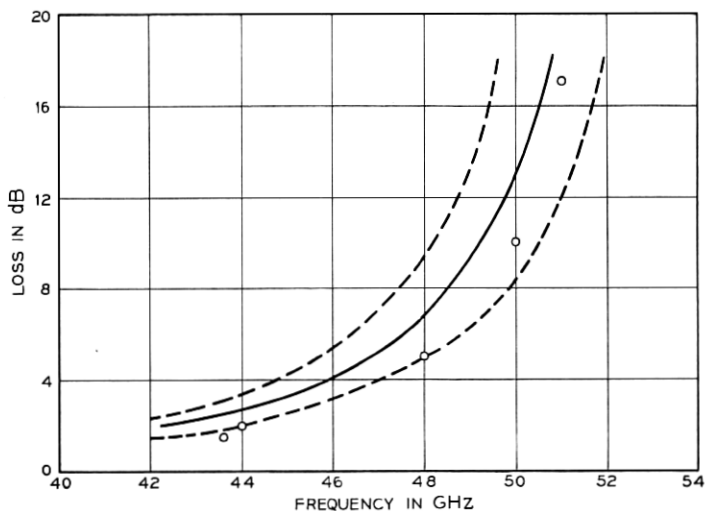
Fig. 8 — Radiation loss as a function of frequency. Dotted lines represent theoretical loss assuming that guide radius is either the maximum or the minimum value. Solid curve shows theoretical loss based on average radius of corrugated rod. The dots are the measured points.
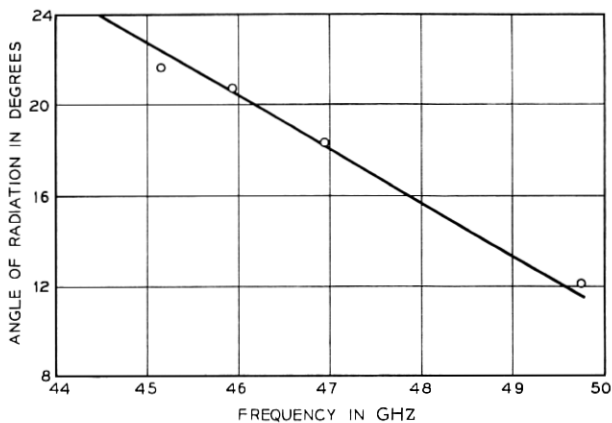

Fig. 9 — The angle of the far-field radiation lobe as a function of frequency. Solid-line represent theory; the dots are measured points.

VII. CONCLUSION

This paper contains a perturbation theory of mode conversion effects and radiation losses of a round dielectric waveguide. This theory is applicable to light transmission in optical fibers. The theory developed here is limited to the circular electric modes of round dielectric waveguides. However, the order of magnitude of the losses for other modes is expected to be similar.

The theory has been checked by a scaled experiment at microwave frequencies. The dielectric fiber with wall imperfections was simulated by a teflon rod of 1 cm diameter which was provided with periodic grooves. Mode conversion from the TE_{01} mode of the dielectric rod to the TE_{02} mode was observed in excellent agreement with experiment. The observed radiation losses are in reasonable agreement with theory. An existing discrepancy can be attributed to the limitations of the perturbation theory to predict correctly the high losses encountered in this experiment.

The conclusion to be drawn from our theory for the operation of optical fibers is a need for very strict tolerance requirements. For example, the radiation losses caused by surface roughness of a fiber designed for single mode operation at 1μ wavelength can be as high as 10 dB/km for an rms variation of the fiber wall of as little as 8 Å.

REFERENCES

1. Marcuse, D., "Mode Conversion Caused by Surface Imperfections of a Dielectric Slab Waveguide," B.S.T.J., this issue, pp. 3187–3215.
2. Marcuse, D., "Radiation Losses of Dielectric Waveguides in Terms of the Power Spectrum of the Wall Distortion Function," B.S.T.J., this issue, pp. 3233–3242.
3. Collin, R. E., *Field Theory of Guided Waves*, New York: McGraw-Hill, 1960.